UC Berkeley
UC Berkeley Previously Published Works

Title

A Versatile Reporter System To Monitor Virus-Infected Cells and Its Application to Dengue Virus and SARS-CoV-2.

Permalink

Journal

ISSN

Authors

Pahmeier, Felix
Neufeldt, Christopher J
Cerikan, Berati
et al.

Publication Date

DOI

Peer reviewed

A Versatile Reporter System To Monitor Virus-Infected Cells and Its Application to Dengue Virus and SARS-CoV-2

Felix Pahmeier,[a] Christopher J. Neufeldt,[a] Berati Cerikan,[a] Vibhu Prasad,[a] Costantin Pape,[b,c] Vibor Laketa,[d] Alessia Ruggieri,[a] Ralf Bartenschlager,[a,d,e] Mirko Cortese[a]

[a]Department of Infectious Diseases, Molecular Virology, University of Heidelberg, Heidelberg, Germany
[b]HCI/IWR, Heidelberg University, Heidelberg, Germany
[c]European Molecular Biology Laboratory, Heidelberg, Germany
[d]German Center for Infection Research, Heidelberg partner site, Heidelberg, Germany
[e]Division "Virus-Associated Carcinogenesis", German Cancer Research Center (DKFZ), Heidelberg, Germany

ABSTRACT Positive-strand RNA viruses have been the etiological agents in several major disease outbreaks over the last few decades. Examples of this include flaviviruses, such as dengue virus and Zika virus, which cause millions of yearly infections around the globe, and coronaviruses, such as SARS-CoV-2, the source of the current pandemic. The severity of outbreaks caused by these viruses stresses the importance of research aimed at determining methods to limit virus spread and to curb disease severity. Such studies require molecular tools to decipher virus-host interactions and to develop effective treatments. Here, we describe the generation and characterization of a reporter system that can be used to visualize and identify cells infected with dengue virus or SARS-CoV-2. This system is based on viral protease activity that mediates cleavage and nuclear translocation of an engineered fluorescent protein stably expressed in cells. We show the suitability of this system for live cell imaging, for visualization of single infected cells, and for screening and testing of antiviral compounds. With the integrated modular building blocks, this system is easy to manipulate and can be adapted to any virus encoding a protease, thus offering a high degree of flexibility.

IMPORTANCE Reporter systems are useful tools for fast and quantitative visualization of virus-infected cells within a host cell population. Here, we describe a reporter system that takes advantage of virus-encoded proteases expressed in infected cells to cleave an ER-anchored fluorescent protein fused to a nuclear localization sequence. Upon cleavage, the GFP moiety translocates to the nucleus, allowing for rapid detection of the infected cells. Using this system, we demonstrate reliable reporting activity for two major human pathogens from the *Flaviviridae* and the *Coronaviridae* families: dengue virus and SARS-CoV-2. We apply this reporter system to live cell imaging and use it for proof-of-concept to validate antiviral activity of a nucleoside analogue. This reporter system is not only an invaluable tool for the characterization of viral replication, but also for the discovery and development of antivirals that are urgently needed to halt the spread of these viruses.

KEYWORDS SARS-CoV-2, dengue virus, live cell imaging, reporter system, reporter cell lines, viral proteases

P ositive-sense single-stranded RNA viruses constitute a major fraction of endemic and emerging human viruses (1). Among the positive-strand RNA viruses, flaviviruses such as dengue virus (DENV) and Zika virus (ZIKV) are some of the most prevalent arboviral pathogens and are considered a major public health problem (2, 3). Currently, there are no universal vaccines or specific antiviral drugs approved for the prevention or

treatment of infections with these viruses (4). Members of the *Coronaviridae* family also have a positive-strand RNA genome and have caused several major outbreaks in the last 2 decades (5, 6). Currently, the world is facing the pandemic outbreak of SARS-CoV-2, the causative agent of coronavirus disease 2019 (COVID-19) (7, 8). As of November 2020, over 54 million confirmed cases and more than 1.3 million confirmed deaths have been reported in 216 countries (9). Despite immense efforts by research teams around the world, there is still a dire need for effective and widely available treatment options and a prophylactic vaccine.

Once released into the cell, the full genome of flaviviruses and the large open reading frame (ORF1ab) of coronaviruses are translated as polyproteins. Signal peptides and internal transmembrane regions direct polyprotein synthesis to the endoplasmic reticulum (ER) membrane, where cotranslational cleavage generates the mature viral proteins (10, 11). The flaviviral protease NS2B/3, together with host proteases, cleaves the flavivirus polyprotein into three structural and seven nonstructural proteins (12). In the case of coronaviruses, ORF1ab is expressed as two polyproteins, which are cleaved into 16 nonstructural proteins (nsp) by the viral papain-like protease (PL$_{pro}$) residing in nsp3 and the 3C-like protease (3CL$_{pro}$) of nsp5 (13–16). The replication of viral RNA for both virus groups occurs on ER-derived membranes, in specialized virus-induced membrane compartments termed replication organelles (10–12, 17, 18).

Reporter systems for detection of virus infection are an invaluable tool for the characterization and quantification of virus infection kinetics, for the characterization of virus-host cell interactions, and for the identification of antiviral compounds. One approach is the insertion of tags into the viral genome that, upon replication and translation, allow for visualization of the infected cells. However, this approach requires functional molecular clones of a given viral genome, which are not always available. In addition, insertion of a tag frequently causes attenuation of viral replication competency and, therefore, the search for adequate insertion sites is time-consuming and often fails.

An alternative approach is the use of engineered fluorescent reporter proteins stably expressed in cells that are altered upon virus infection (19–21). Building on this idea, we established a reporter system based on an ER-anchored green fluorescent protein (GFP) that, upon recognition and cleavage of a specific linker region by a viral protease, is released from the ER and translocated to the nucleus. Using this system, we demonstrate reliable reporting activity for DENV and SARS-CoV-2 infected cells. Moreover, we have applied this reporter cell system to live cell imaging and the assessment of an antiviral compound.

RESULTS

Design and characterization of DENV reporter constructs. In order to generate a reporter system that can specifically indicate virus infection, we designed a construct to express a GFP fusion protein that could be selectively cleaved by viral proteases. The reporter construct was engineered for viruses that produce ER-tethered polyproteins that are processed by viral proteases in close proximity to ER membranes. The transmembrane (TM) domain of the ER resident protein sec61β was used to target the reporter protein to ER membranes (Fig. 1). This ER anchor was connected to a GFP moiety containing the simian virus 40 (SV40) large T-antigen nuclear localization signal (NLS) sequence via a variable linker. The linker region was flanked by restriction enzyme recognition sites, allowing the easy insertion and screening of different protease cleavage sequences (Fig. 1A). Protease cleavage of the linker would result in GFP translocation from the cytosolic ER to the nucleus, which can be easily detected and quantified by light microscopy.

The DENV polyprotein is cleaved into the individual viral proteins by either the host signal peptidase or the viral NS2B/3 serine protease (22, 23). The ER-resident NS2B protein acts as a cofactor of NS3 protease and anchors it to ER membranes (24, 25). To
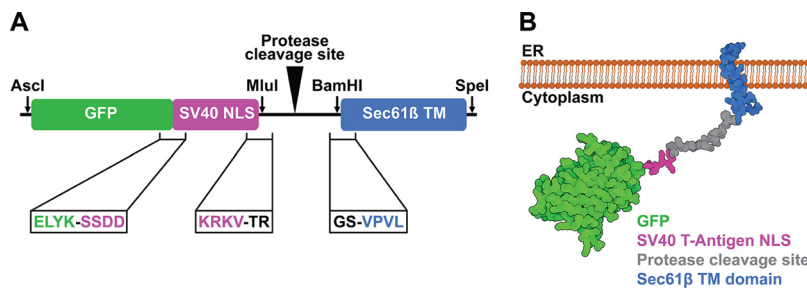
FIG 1 Schematics of the reporter construct (A) and the predicted membrane topology (B). (A) Arrows indicate the restriction sites for MluI and BamHI that flank the linker region and allow the insertion of the protease cleavage site. Amino acid sequences flanking the junctions of the different modules are given in the boxes. (B) Proteins and peptides are colored as indicated on the bottom right of the panel.

determine an optimal system for reporting DENV infection, several previously described NS2B/3 specific cleavage sequences were inserted into the reporter construct (Table 1).

Reporter cell lines for each of the constructs were generated by lentiviral transduction of Huh7 cells at an MOI of 5 to ensure maximal transduction efficiency. Subsequently, the cell pools expressing an individual construct were infected with DENV2 for 48 h (MOI = 5). Reporting activity for each cell line was tested by assessing the subcellular GFP localization by indirect immunofluorescence (IF) in infected versus noninfected cells. To ensure specificity of GFP translocation, cells were fixed and stained for DENV2 NS3 protein.

In DENV2 infected-cells, NS3 was observed in the perinuclear region as previously described (10, 17, 26). In uninfected cells, the GFP signal from cells expressing the reporter constructs 1, 2, 3, and 7 showed an ER-like pattern, while cells expressing constructs 4, 5, 6, and 8 already showed nuclear GFP signal in the absence of DENV2 (Fig. 2A and B). In infected cells expressing reporter construct 1, a noticeable increase of nuclear GFP signal was observed (Fig. 2C). Similar nuclear GFP accumulation was also observed in reporter cell lines expressing constructs 3, 4, 5, 7, and 8 upon DENV2 infection. No clear differences in GFP localization were seen for constructs 2 and 6 following virus infection. Among all the tested constructs, construct 1 showed the highest number of cells that were double positive for nuclear GFP signal and NS3 staining, with only ~6% of cells positive for NS3 staining alone (Fig. 2C and D).

To further investigate cleavage of the reporter proteins in DENV2-infected cells, we used Western blot analysis of cell lysates prepared 48 h postinfection (hpi) (Fig. 2E). Based on the construct design, the uncleaved GFP-NLS fusion protein was predicted to have a molecular weight of ~34 kDa. In the uninfected cells, we observed a GFP protein with the expected molecular weight and an additional band with an apparent lower molecular weight (Fig. 2E, left panel). Upon DENV2 infection, additional ~30 kDa GFP antibody-reactive proteins were detectable in lysates of cells transduced with reporter constructs 1, 4, 5, and 7, and, to a lesser extent, in lysates of cells transduced with constructs 3 and 8. This is consistent with the predicted molecular weight of the

TABLE 1 List of DENV cleavage site sequences inserted into the reporter construct

No.	Name	Cleavage site sequence[a]	Source
1	Capsid	RRRR↓SAGM	(51)
2	DV$_{opt}$	GKKRR↓PVK	(51)
3	NS2AB	SKKR↓SWPL	(51)
4	NS2B3	KKQR↓AGVL	(51)
5	NS3hel	AQRR↓RRIG	(51)
6	NS3prohel	RKRR↓LTIM	(51)
7	panFlav	GLKR↓GGAK	(51)
8	ZV$_{opt}$	KTGKR↓SGAL	(34)

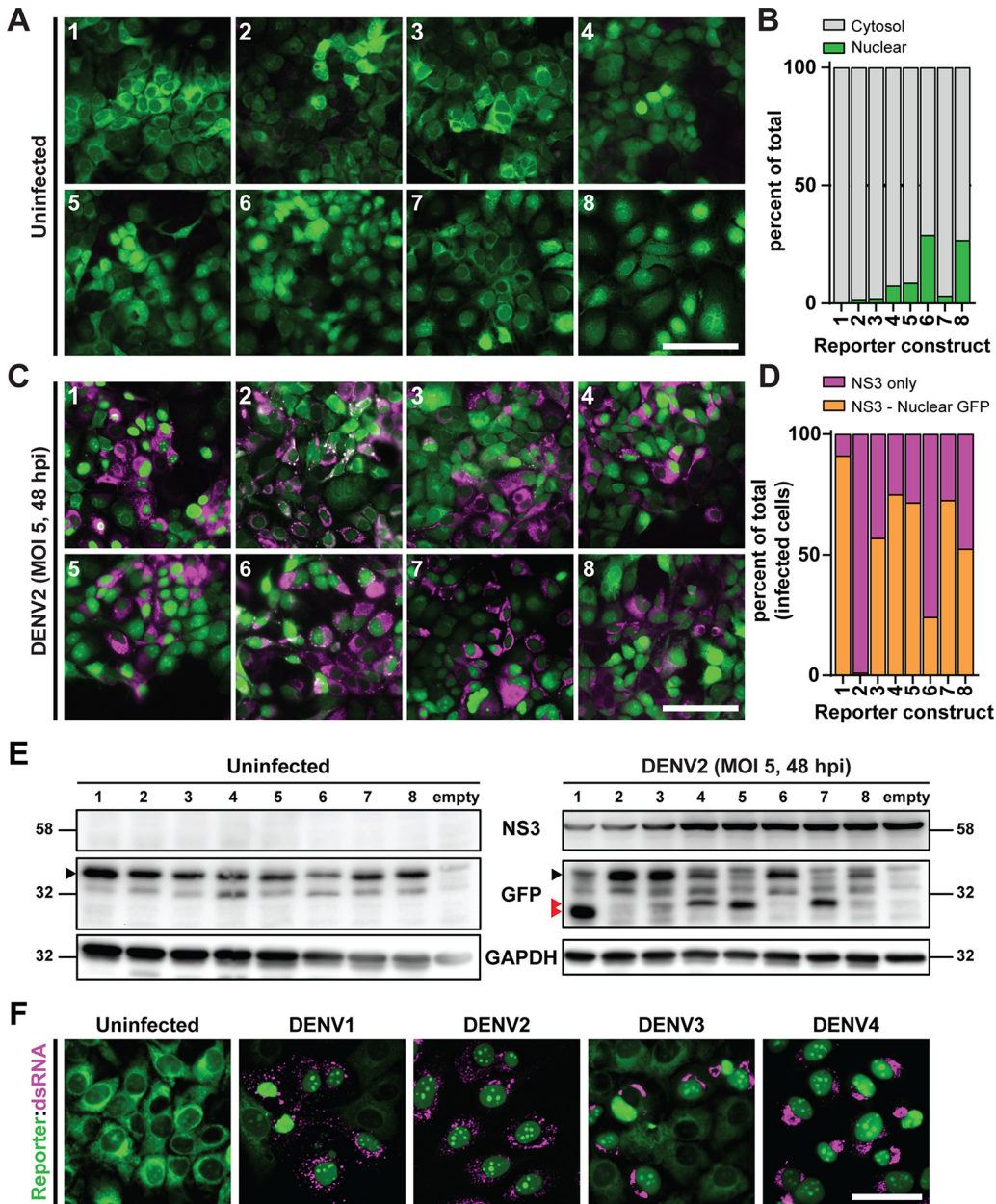[a]Cleavage site is indicated with ↓.

FIG 2 Evaluation of DENV reporter constructs. (A) Huh7 cells were transduced with lentiviruses encoding the different DENV GFP-based reporter constructs 1 to 8 (Table 1) at an MOI of 5. Cells were fixed at 72 h posttransduction and the subcellular distribution of GFP was analyzed by confocal microscopy. Scale bar = 100 μm. (B) Quantification of images acquired as in panel A. The percentage of cells showing nuclear or cytosolic GFP localization is shown. For each construct, more than 70 cells were counted. (C) Huh7 cells were transduced as above for 24 h before being infected with DENV2 at an MOI of 5. Cells were fixed at 48 hpi and NS3 was stained by immunofluorescence. Samples were analyzed by confocal microscopy. Magenta, DENV NS3 protein; green, reporter GFP signal. Scale bar = 100 μm. (D) Quantification of images as in panel C. The percentages of cells positive for NS3 and positive for both nuclear GFP and NS3 signals were quantified. For each construct, more than 60 cells were counted. (E) Cells expressing the reporter constructs 1 to 8 or an empty plasmid (empty) were infected with DENV2 (MOI = 5). At 48 hpi, cells were lysed and 10 μg of total protein for each sample was resolved by SDS-PAGE. NS3 and GFP were detected with a specific antibody. Glyceraldehyde-3-phosphate dehydrogenase (GADPH) served as a loading control. Black arrowheads, uncleaved reporter; red arrowheads, reporter cleavage products. (F) Huh7-derived cells expressing reporter construct 1 (Huh7-RC) were infected with DENV serotypes 1 to 4 at an MOI of 5. Cells were fixed at 48 hpi and stained for double-stranded RNA (dsRNA) by IF. GFP and dsRNA signals were detected by fluorescence microscopy. For each serotype, more than 200 cells from at least two fields of view in duplicate were screened. Scale bar = 50 μm.

cleavage product. However, we noted that the cleavage product obtained from lysates expressing construct 1 had an apparent molecular weight slightly lower than expected. This difference could be due to the amino acid sequence at the C terminus of the cleavage product or further trimming by cellular enzymes.

With the aim to evaluate the suitability of this reporter system for the other DENV serotypes, we focused on reporter construct 1, which gave the best results with respect to cleavage and nuclear translocation of the GFP cleavage product. Huh7 cells transduced with this reporter (designated Huh7-RC) were infected with DENV strains corresponding to the 4 different serotypes and infection was monitored by immunostaining of double-stranded RNA (dsRNA), an intermediate of viral genome replication (Fig. 2F). In all cases, we observed a strong correlation between dsRNA staining and nuclear accumulation of GFP, showing that the reporter system is broadly applicable for all DENV serotypes.

Time-course experiments confirm early and reliable identification of DENV- and NS2B/3-positive cells. Next, we analyzed the kinetics of GFP translocation in the Huh7-RC reporter cell line. Cells were infected with either the wild-type (WT) DENV2 or with a recombinant DENV reporter expressing a far-red fluorophore (DENV-faR; MOI = 5) (27). Cells were fixed at 24 h, 48 h, or 72 h postinfection and subsequently analyzed by wide-field fluorescence microscopy (Fig. 3A).

Uninfected reporter cells exhibited the predicted ER-like localization of the GFP signal. In contrast, reporter cells infected with WT virus showed nuclear GFP localization as early as 24 h after infection, and the proportion of cells showing nuclear signal increased at later time points (Fig. 3A). Reporter cells infected with DENV-faR showed a similar trend, although a lower number of reporting cells was observed at 24 h and 48 h postinfection in comparison to WT-infected reporter cells (Fig. 3A), consistent with lower replication capacity of the reporter virus (27). Cells infected with DENV-faR showed an increase of red fluorescence signal in a time-dependent manner, providing evidence for viral replication and spread. Importantly, ~83 to 100% of cells exhibiting red fluorescence also showed nuclear translocation of GFP at 48 h or 72 h postinfection, respectively (Fig. 3B). Additionally, only 2 to 3% of cells were positive for nuclear GFP in the absence of reporter virus signal.

To assess the correlation of nuclear GFP translocation and viral replication kinetics, reporter cells were infected with DENV2 and viral replication was monitored by IF staining of dsRNA at different time points after infection. As shown in Fig. 3D, the percentage of dsRNA-positive cells correlated well with the percentage of cells showing nuclear GFP across the different time points (Fig. 3D). These results demonstrate that the reporter system allows for reliable detection of DENV-infected cells at different time points after infection without the need for fixation and intracellular staining.

Live cell imaging of cells expressing the DENV polyprotein. Recently, a plasmid-based expression system for induction of DENV replication organelles in transfected cells has been described (28). This system, designated plasmid-induced replication organelle-dengue (pIRO-D), encodes the viral polyprotein that is translated from an RNA generated in the cytoplasm by a stably expressed T7 RNA polymerase. In this way, the pIRO-D system allows the analysis of viral proteins in cells, independent of viral replication. However, since no fluorescent protein coding sequence is incorporated into the construct, expression of the DENV polyprotein cannot be followed by live cell imaging.

To overcome this limitation, we determined whether our DENV reporter cell line could be combined with the pIRO-D system to analyze the expression of the viral polyprotein in real time. Huh7-Lunet cells stably expressing the T7 RNA polymerase and the reporter construct 1 (Lunet-T7-RC) were seeded in dishes with glass bottoms and on the next day transfected with the pIRO-D construct (Fig. 3E). The growth medium was changed to imaging medium at 4 h after transfection and the dishes transferred to a live cell imaging microscope. The GFP signal was recorded every 10 min for 8 h (final time point at 12 h posttransfection). Representative images of mock-transfected and pIRO-D-transfected cells at 2 h increments are shown in Fig. 3F; a video spanning
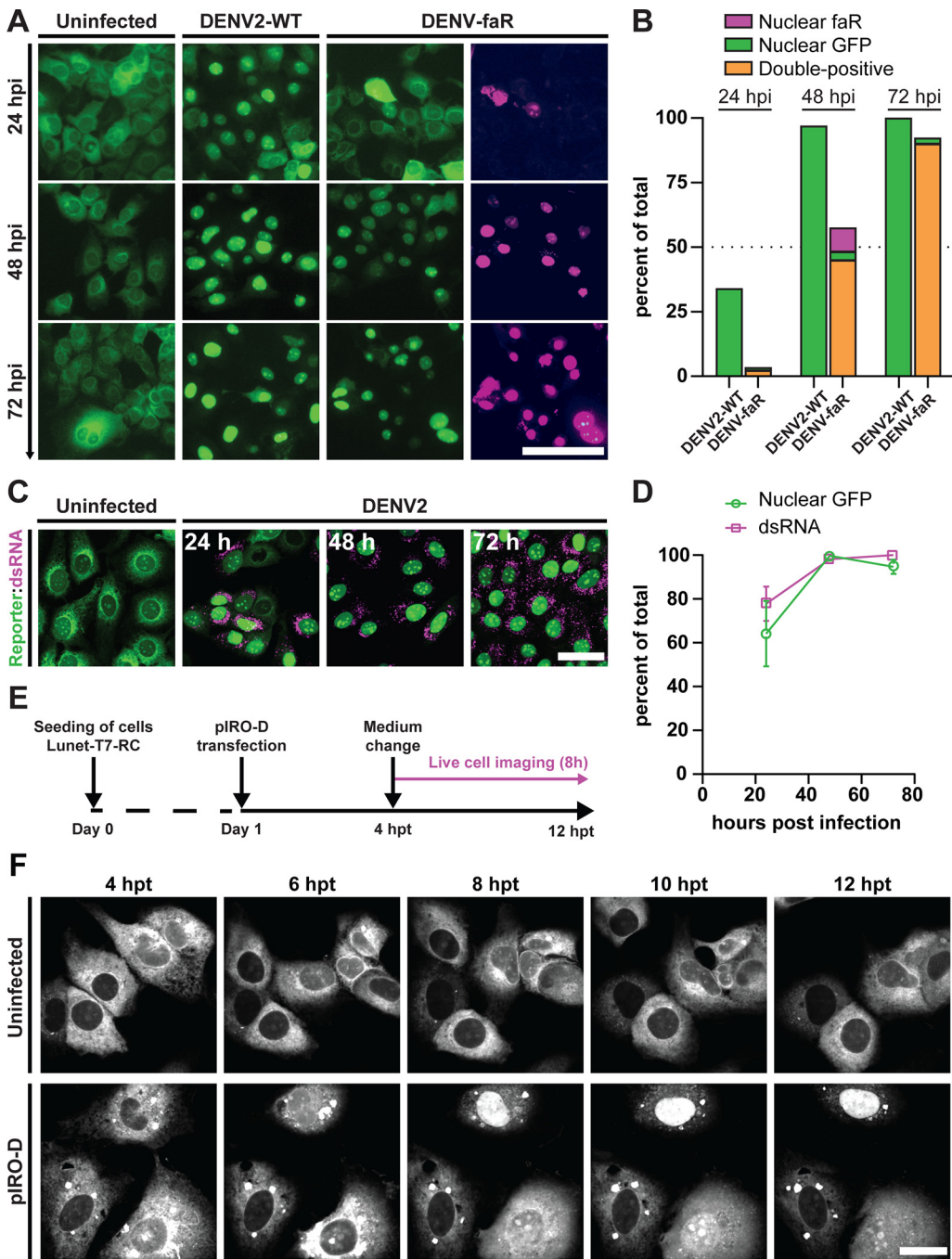
FIG 3 Time-course experiments using the DENV reporter system in infection and transfection settings. (A) Huh7 cells stably expressing the reporter construct 1 were infected with DENV2 WT, the reporter virus DENV-faR (MOI = 5), or left uninfected. Cells were fixed at the indicated time points postinfection (hpi) and signals of the reporter virus (magenta) and the GFP-based reporter construct (green) were detected with a wide-field fluorescence microscope. Scale bar = 100 μm. (B) Quantification of images acquired as in panel A. The percentages of cells positive for nuclear GFP signal (Nuclear-GFP), DENV-faR reporter virus (Nuclear-faR), and double positive for both nuclear GFP and faR reporter signals (orange) were quantified. For each time point, more than 50 cells were analyzed. Values were normalized by setting the total number of cells counted using DAPI staining to 100%. (C) Huh7 cells stably expressing the reporter construct 1 were infected with DENV2 (MOI = 5). Cells were fixed at the indicated hpi and viral double-stranded RNA (dsRNA) was stained by IF. dsRNA (magenta) and GFP (green) signals were detected by confocal microscopy. Scale bar = 50 μm. (D) Quantification of cells using acquired images from the experiment shown in panel C. Percentages of cells positive for the nuclear GFP signal (green) and dsRNA (magenta) were quantified. For each time point, more than 250 cells were counted. Values were normalized by setting the total number of cells as determined by DAPI staining to 100%. (E) Experimental set-up to monitor GFP-reporter activation in pIRO-D transfected live cells. (F) Lunet-T7-RC cells stably expressing the T7 RNA polymerase and the reporter construct 1 were mock- or pIRO-D-transfected. Four hours after transfection, the medium was changed and live cell imaging was performed for 10 h using a confocal spinning disc microscope. Images of representative fields of view and the indicated time points are shown. Scale bar = 20 μm. See also Movie S1 in the supplemental material.

TABLE 2 List of SARS-CoV cleavage site sequences inserted into the reporter construct

No.	Name	Cleavage site sequence[a]	Protease[b]
1	nsp1/2	ELNGG↓AVTR	PL$_{pro}$
2	nsp2/3	RLKGG↓APIKG	PL$_{pro}$
3	nsp3/4	SLKGG↓KIVST	PL$_{pro}$
4	nsp4/5	SAVLQ↓SGFRK	3CL$_{pro}$
5	nsp5/6	GVTFQ↓GKFKK	3CL$_{pro}$
6	nsp6/7	VATVQ↓SKMSD	3CL$_{pro}$
7	nsp7/8	RATLQ↓AIASE	3CL$_{pro}$
8	nsp8/9	AVKLQ↓NNELS	3CL$_{pro}$
9	nsp9/10	TVRLQ↓AGNAT	3CL$_{pro}$
10	nsp10/RdRp	EPLMQ↓SADAS	3CL$_{pro}$
11	RdRp/Hel	HTVLQ↓AVGAC	3CL$_{pro}$
12	Hel/nsp14	VATLQ↓AENVT	3CL$_{pro}$
13	nsp14/15	FTRLQ↓SLENV	3CL$_{pro}$
14	nsp15/16	LQASQ↓AWQPG	3CL$_{pro}$

[a]Cleavage site is indicated with ↓.
[b]PL$_{pro}$, papain-like protease/nsp3; 3CL$_{pro}$, 3C-like protease/nsp5.

an 8 h observation period of transfected cells is shown in Movie S1 in the supplemental material.

No nuclear translocation of the GFP reporter was detected in mock-transfected Lunet-T7-RC cells (Fig. 3F, upper row). In pIRO-D-transfected cells, in contrast, nuclear localization was already detectable in cells as early as 4 h posttransfection, suggesting a robust expression of the viral polyprotein. The number of cells with nuclear GFP signal, as well as the intensity of the nuclear signal, increased over time.

Development of a reporter system for identification of SARS-CoV-2-infected cells. The recent outbreak of SARS-CoV-2 has created a dire need for tools to characterize virus infection and develop therapeutics. Therefore, we adapted and optimized our reporter system for the detection of SARS-CoV-2 infection. The first two open-reading frames of coronaviruses are expressed as polyproteins ORF1a/b which are cleaved into the individual proteins by viral proteases PL$_{pro}$ and 3CL$_{pro}$ (13–15). The sequence of the SARS-CoV-1 Frankfurt isolate was analyzed to determine the protease cleavage sites between individual nsps, and the deduced sequences were inserted into the linker region of our reporter construct (Table 2). The generation of constructs 2, 11, and 13 failed at the cloning stage and they were not further pursued.

Cells expressing the GFP reporter containing the individual cleavage site linkers were generated by lentiviral transduction of A549 cells stably expressing the SARS-CoV-2 receptor ACE2 (A549-ACE2) (29). Productive infection of the cells with SARS-CoV-2 (strain BavPat1) was determined by detection of dsRNA at 48 h postinfection. Cytosolic GFP localization was observed in all uninfected cells expressing the reporter constructs except for construct 3, where nuclear signal was evident (Fig. 4A and B). No clear differences in GFP localization between uninfected and virus-infected cells were observed for reporter constructs 1, 5, and 7 (Fig. 4C), arguing for inefficient cleavage, perhaps because of poor accessibility of the cleavage site outside the context of the authentic viral polyprotein. For all the other constructs, we detected an increase in nuclear GFP signal upon infection, with the reporter construct 14 cell line showing the highest number of cells positive for both dsRNA and nuclear GFP (Fig. 4C and D). Therefore, we used the cell line expressing construct 14 for the further development of our SARS-CoV-2 reporter system.

Since transiently transduced cells expressing the SARS-CoV-2 reporter construct showed highly heterogeneous GFP signal intensity and large fluorescent aggregates (Fig. 4A and C), we generated single cell clones by FACS sorting for cells with low total GFP signal. Among the 20 cell clones generated, clone C2 was selected based both on SARS-CoV-2 infection susceptibility and reporting activity (data not shown). SARS-CoV-2 infection of this A549-ACE2 reporter cell clone showed a time-dependent increase in nuclear GFP translocation events that highly correlated with the increase
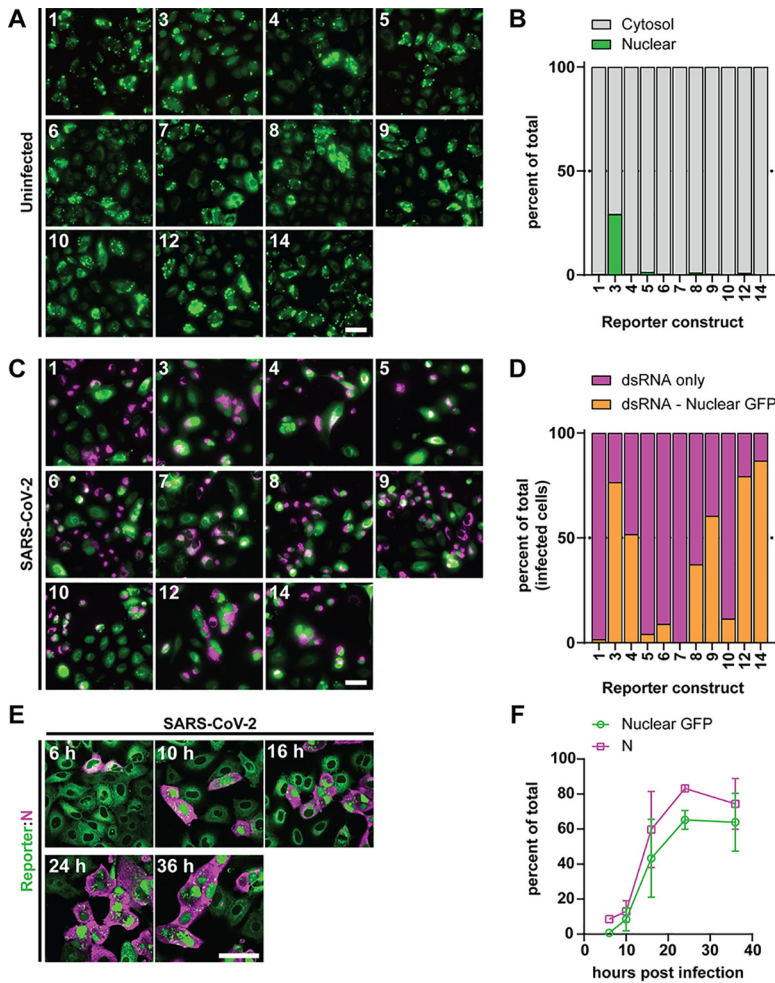
FIG 4 Screening of SARS-CoV-2 reporter constructs. (A) A549-ACE2 cells were transduced with lentiviruses encoding the reporter constructs specified on the top left of each panel. Cells were fixed at 32 h posttransduction and GFP localization was analyzed using a wide-field fluorescence microscope. (B) Quantification of images acquired as in panel A. The percentages of nuclear or cytosolic GFP are shown (green and gray, respectively). At least 290 cells were counted for each construct. (C) Cells transduced as in panel A were infected with SARS-CoV-2 (MOI = 5) at 16 h posttransduction. Cells were fixed at 16 hpi and dsRNA (magenta) and the GFP-based reporter construct (green) were detected by immunofluorescence using a wide-field fluorescence microscope. (D) Quantification of images acquired as in panel C. Percentages of infected cells positive for dsRNA only (magenta) or double positive for nuclear GFP signal and dsRNA (orange) are shown. For each construct, more than 85 cells were counted. Scale bars = 50 μm. (E) A549-ACE2 cells stably expressing reporter construct 14 were infected with SARS-CoV-2 (MOI = 10). Cells were fixed at the indicated time postinfection (top left corner) and the SARS-CoV-2 N protein was stained by IF. N protein (magenta) and GFP (green) subcellular distributions were determined by confocal microscopy. Scale bar = 50 μm. (F) Quantification of the acquired images as described for panel E. Percentages of cells with N protein staining (magenta) and nuclear GFP signal (green) are shown for the different time points. For each time point more than 190 cells were analyzed.

in cells positive for the viral N protein (Fig. 4F). Thus, the newly established reporter cell line allowed for robust detection of SARS-CoV-2-infected cells and viral replication kinetics.

Live cell imaging of SARS-CoV-2 infection. Previous studies have determined that a complete virus replication cycle can occur within 6 h after infection, but that virus replication and assembly continues to increase up to 24 h in A549-ACE2 cells (29). To characterize the dynamics of SARS-CoV-2 infection in the A549-ACE2 reporter cell clone, we performed live cell imaging (Fig. 5A). Imaging was started at 2 h postinfection and images were acquired every 10 min for 18 h (final time point 20 h
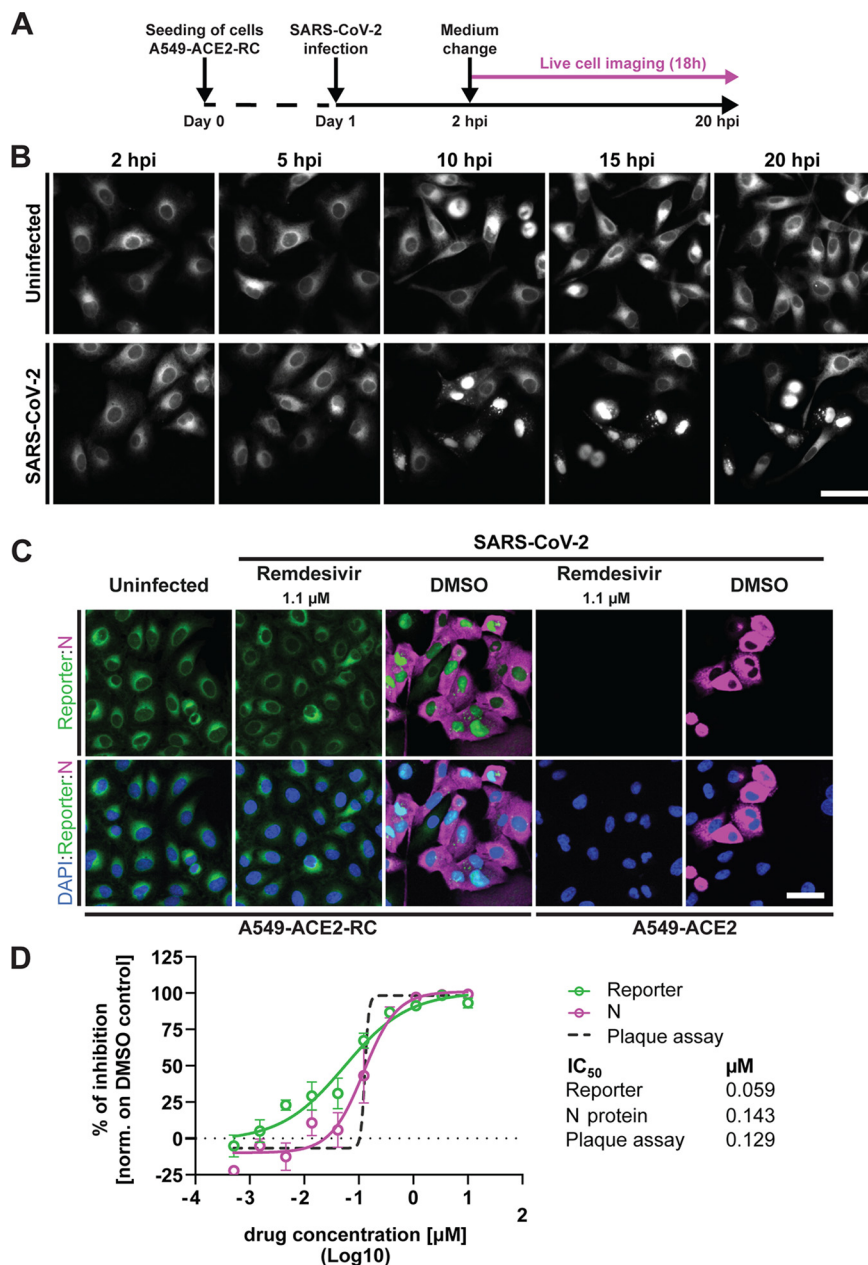
FIG 5 Application of the SARS-CoV-2 reporter cell line for live cell imaging of viral infection and assessment of antiviral activity of remdesivir. (A) Experimental setup to monitor GFP-reporter activation in SARS-CoV-2-infected cells. (B) A549-ACE2-RC cells (clone C2) stably expressing the reporter construct 14 were infected with SARS-CoV-2 (MOI = 10). At two hours postinfection (hpi), live cell imaging was performed for 18 h using a confocal spinning disc microscope. Images of representative fields of view and time points are displayed. Scale bar = $50\,\mu$m. (C) A549-ACE2 and A549-ACE2-RC (clone C2) expressing the SARS-CoV-2 reporter construct 14 were incubated with remdesivir ($1.1\,\mu$M) or DMSO only and infected with SARS-CoV-2 (MOI = 5). After 16 h, cells were fixed and stained for N protein prior to imaging with a confocal spinning disc microscope. Scale bar = $50\,\mu$m. (D) IC_{50} calculation of remdesivir in reporter cell clone 2 infected with SARS-CoV-2 (MOI = 5). Percentages of inhibition were calculated by quantification of the number of N-positive cells and cells with nuclear GFP signal in duplicate wells for each compound concentration. Values were normalized by setting the average number of infected cells in the DMSO-treated sample as 0% inhibition.

postinfection) (Movie S2). Representative images of uninfected and SARS-CoV-2-infected cells are shown in Fig. 5B. Uninfected cells exhibited an ER-like GFP signal throughout the observed time frame. In infected cells, a time-dependent increase in the numbers of cells showing nuclear GFP signal was observed, with the earliest

translocation event starting at 5.5 h postinfection (Movie S2). These data demonstrate the suitability of our reporter system for live cell imaging analysis of SARS-CoV-2 infection.

Application of the SARS-CoV-2 reporter for drug screening. The need for effective treatment of COVID-19 prompted us to investigate the suitability of the reporter cell line for drug screening. A proof-of-concept experiment was performed using the nucleoside analogue remdesivir, which is currently the only FDA-approved drug for treatment of SARS-CoV-2 infection. Both the A549-ACE2 C2 reporter clone and the parental A549-ACE2 cells without reporter construct expression were incubated with serial dilutions of remdesivir for 30 min and infected with SARS-CoV-2 (MOI = 5). The compound remained present throughout the duration of the experiment. Cells were fixed at 16 h postinfection and GFP translocation was evaluated using confocal microscopy.

Treatment with 1.1 μM remdesivir reduced viral N protein fluorescence signal in both cell lines below the detection limit, confirming the previously described antiviral activity of this nucleoside analogue (30, 31) (Fig. 5C). Nuclear GFP signal was observed in dimethyl sulfoxide (DMSO)-treated reporter cells infected with SARS-CoV-2, confirming the reporting activity of the cell line. The percentage of cells displaying nuclear GFP signal and cytosolic N protein staining in the different remdesivir dilutions was quantified by semiautomated image analysis workflows (32, 33) (Fig. 5D). The 50% inhibitory concentration (IC_{50}) calculated for the N protein staining was 143 nM, in line with the IC_{50} values calculated by plaque assay (IC_{50} = 129 nM). Quantification using the reporter signal gave an IC_{50} of 59 nM. This decrease in IC_{50} value is likely due to reduced sensitivity of the reporter construct that relies on $3CL_{pro}$ activity and the higher background in the readout in comparison to IF staining of the highly abundant N protein. Nevertheless, the two IC_{50} values differ by only a factor of $\sim$3 and therefore are quite comparable. Thus, our reporter system can be reliably used in primary screens of large compound libraries.

DISCUSSION

This study describes the generation and characterization of a fluorescence-based reporter system for detection of DENV and SARS-CoV-2 infection. The reporter construct contains three functional elements: (i) a fluorescent protein fused to an NLS, (ii) the TM domain of sec61β for ER membrane anchoring, and (iii) an exchangeable protease cleavage site cassette located within the linker region that connects the fluorescent protein and the ER anchor. This design allows easy adaptation of the reporter system to other viruses that encode specific viral proteases, especially for other positive-stranded RNA viruses replicating in the cytoplasm. The high selectivity and specificity of the constructs, as shown by IF, Western blotting, and live cell imaging, render this tool suitable for applications that require single-cell analysis, such as live cell imaging and correlative light-electron microscopy (CLEM) approaches. Moreover, combining our reporter cell lines with image analysis pipelines that quantify nuclear translocation events allows for rapid and robust assessment of antiviral efficacy of compounds or other antiviral interventions, including high-throughput screening of large compound libraries.

Among the different cleavage sites tested for DENV, reporter construct 1, composed of the cleavage site between capsid and prM, allowed reliable and selective identification of infected or transfected cells with a construct expressing the viral polyprotein (Fig. 2 and 3). Interestingly, for several DENV reporter constructs, nuclear GFP localization was observed in the absence of the viral protease (Fig. 2A). A possible explanation for this could be that unspecific cleavage of the linker region might be mediated by cellular proteases due to high levels of expression of the reporter construct upon transient transduction.

Reporter constructs for detection of flavivirus infection have been described previously which were either cytosolic or employed viral nonstructural proteins as ER anchors (19–21, 34). Most of these reporter systems rely on the expression of large

fragments of viral proteins (19–21) which can alter the physiological stoichiometry of the viral proteins and induce undesired pleiotropic effects. Indeed, even expression of single NS proteins can affect cellular functions, such as alteration of mitochondrial morphodynamics by NS4B (35). In contrast, since our reporter construct does not contain viral sequences, except for the cleavage site, it is less prone to affect cellular or viral pathways and processes.

The flexibility granted by the modular nature of our constructs allows for simple adaptation of the reporter system to different viruses that encode proteases acting in close proximity to the ER membranes. This allowed us to rapidly adapt the system for the detection of SARS-CoV-2 infection in cell culture. Transient transduction of cells with lentiviruses coding for the different constructs allowed fast screening and identification of the most suitable cleavage site (Fig. 4). Notably, while it was sufficient to use cell pools under antibiotic selection for DENV reporter cell lines Huh7-RC and Lunet-T7-RC, we had to establish single-cell clones for the SARS-CoV-2 reporter proteins because, in most cells, large fluorescent aggregates were observed (Fig. 4A). This is likely due to differences in the ability of cell lines to respond to high levels of GFP fusion proteins. In addition to sorting for cells with lower reporter expression, as done here, this problem might be overcome by employing promoters with lower transcriptional activity or by using alternative fluorescent proteins.

Live cell imaging demonstrated that SARS-CoV-2-infected cells can be identified as early as 5.5 h postinfection (Movie S2 in the supplemental material). Real-time identification of SARS-CoV-2-infected cells is currently performed mainly by employing recombinant viruses expressing reporter genes (36–38). While these studies report robust and reliable identification of infected cells, our reporter cell line has advantages in certain settings. The use of reporter viruses requires molecular clones and the adaptation of the genomic sequence for each different isolate, which, for viruses with large RNA genomes like SARS-CoV-2, involves substantial cloning efforts. Additionally, the relatively high mutation and recombination rate of RNA viruses during genome replication makes reporter viruses inherently unstable. Moreover, integration of a reporter gene into the recombinant virus may attenuate the replication efficiency, as observed when comparing WT to DENV-faR virus infection (Fig. 3B). In contrast, our cell line allows the detection of wild-type virus isolates, although conserved cleavage site sequences are required in this system.

We tested the suitability of the SARS-CoV-2-optimized reporter cell line to assess the antiviral activity of remdesivir and determined an IC_{50} of 59 nM in our reporter system. By using N staining as an alternative readout, we obtained a somewhat lower efficacy of remdesivir (IC_{50} = 143 nM) which is closer to the data reported in the literature (30, 31, 39). The reduced sensitivity of the reporter construct, which relies on $3CL_{pro}$ activity and GFP translocation, might stem from a failure to detect cells with low levels of infection, whereas the highly expressed N protein is already detectable by IF. Additionally, the selected cell clone 2 might differ in remdesivir metabolism, which can impact the antiviral efficacy of the nucleoside analogue. It is important to note that the IC_{50} value varies depending on which cell lines and assays are employed, and the IC_{50} values determined in this study are in a similar range with only a 3-fold difference. Nevertheless, compounds found to exhibit antiviral activity in our reporter construct should be further validated by methods such as plaque assay and/or viral RNA level quantification. Therefore, the reporter cell line can be employed in a primary screen to lower the number of candidates for validation in more sophisticated and time-consuming assays, thus reducing costs and increasing speed.

Two additional applications of our system shall be mentioned. The first is the use for CLEM, a powerful imaging method that can be used to mark and identify cells of interest among a large number of noninfected or untransfected cells, and subsequently analyze traced cells by electron microscopy (40). Second, the reporter cell line described here can also be employed for protease inhibitor screens in areas that do not have access to biosafety level 3 laboratories. This can be done by transient or

TABLE 3 List of antibodies used in this study

| Antibody | Concentration[c] | | Source |
	WB	IF	
Mouse IgG1 anti-DENV NS3[a]	1:1,000	1:200	GeneTex
Mouse anti-GAPDH[a]	1:1,000		Santa Cruz Biotechnology
Rabbit anti-GFP[a]	1:1,000		Roche
Mouse IgG2a anti-dsRNA[a]		1:400	Scicons
Mouse IgG1 anti-SARS-CoV N[a]		1:500	Sino biologicals
Goat anti-mouse IgG-HRP[b]	1:10,000		Sigma
Goat anti-rabbit IgG-HRP[b]	1:10,000		Sigma
Alexa Fluor 568 donkey anti-mouse IgG[b]		1:1,000	Thermo Fisher Scientific
Alexa Fluor 568 donkey anti-rabbit IgG[b]		1:1,000	Thermo Fisher Scientific

[a]Primary antibody.
[b]Secondary antibody.
[c]WB, western blot; IF, immunofluorescence.

stable expression of the protease individually and monitoring of the reduction of nuclear GFP as a result of protease inhibition, similar to a recent study (41).

In conclusion, we describe a reporter system suitable for the detection of DENV- and SARS-CoV-2-infected cells. The system is easy to handle and flexible and should be applicable to any virus encoding a cytoplasmic protease. It is suitable for a large number of methods and assays, including high content screening. In all these respects, we expect this tool to facilitate investigations of virus-host interactions, but also the development of antiviral drugs that are urgently needed to curb pandemic viruses such as SARS-CoV-2.

MATERIALS AND METHODS

Cell lines and virus strains. HEK-293T, A549, and VeroE6 cells were purchased from ATCC; Huh7 cells (42) were obtained from Heinz Schaller (Center for Molecular Biology, Heidelberg). Generation of the cell lines Huh7-Lunet and the derivative Huh7-Lunet-T7, stably expressing the RNA polymerase of bacteriophage T7, have been previously described (43, 44). All cells were cultured at 37°C and 5% CO_2 in Dulbecco's modified Eagle medium (DMEM, Life Technologies) containing 10% fetal bovine serum, 100 U/ml penicillin, 100 μg/ml streptomycin, and 1% nonessential amino acids (complete medium). Huh7-Lunet-T7 cells were cultured in complete medium, supplemented with 5 μg/ml zeocin.

Wild-type (WT) DENV2 was produced from an infectious molecular clone based on strain 16681, as described elsewhere (45). DENV serotype 1 (strain Hawaii), DENV serotype 3 (strain H87), and DENV serotype 4 (strain H241) viruses (kindly provided by Progen Biotechnik GmbH, Germany) were amplified in C6/36 insect cells and titers were determined by plaque assay. The DENV reporter virus genome encoding the Turbo fluorescent protein 635 (DENV-faR) has been described previously (27). SARS-CoV-2 (strain BavPat1) was kindly provided by Christian Drosten (Charité, Berlin, Germany) through the European Virology Archive. For the generation of virus stocks, VeroE6 cells were infected with the different viruses. Supernatants were harvested, filtered, and virus concentration was determined by plaque assay. For infection experiments, cells were inoculated as specified in the results section for 1 h at 37°C. Fresh complete medium was then added, and cells were incubated for the indicated time spans.

Virus titration. Titers of infectious virus were assessed by semisolid plaque assay. Briefly, VeroE6 cells were inoculated with serially diluted filtered supernatants harvested from virus-infected cells. One hour postinfection, medium was replaced with plaque medium containing 1.5% or 0.8% carboxymethyl-cellulose in MEM (Life Technologies) for DENV and SARS-CoV-2, respectively. The cells were fixed by addition of formaldehyde (5% final concentration) to SARS-CoV-2- or DENV2-infected cells at 3 or 7 days after infection, respectively. Cell monolayers were stained for 15 min with crystal violet (1%) dissolved in 10% ethanol. After extensive washing, plaques were counted and titers calculated, taking dilutions into account.

Antibodies. The antibodies used in this study are listed in Table 3.

Generation of the reporter construct. A synthetic DNA construct containing the sequence encoding the reporter protein was generated by Integrated DNA technologies (Coralville, IA, USA). The reporter sequence was inserted into the lentiviral vector pWPI via AscI and SpeI restriction sites (pWPI-RC). Oligonucleotides encoding the protease cleavage sites were designed to allow insertion into the vector via MluI and BamHI restriction sites. The primer pairs (Table 4) spanning a given protease cleavage site were heated to 95°C and allowed to anneal by decreasing the temperature in 5°C increments every 2 min. The resulting double-stranded DNA product was inserted via MluI and BamHI into pWPI-RC and ligation products were amplified in *Escherichia coli* (strain DH5α). Integrity of amplified plasmids was

TABLE 4 Sequences of oligonucleotides used in this study

No.	Name	Sequence (5′–3′)[a]	Orientation[b]
1	Capsid	CGCGTaggagacgcagatctgccggcatgg	fwd
2		gatcccatgccggcagatctgcgtctcctA	rvs
3	DV$_{opt}$	CGCGTggaaagaaaagaagaccagtaaagg	fwd
4		gatccctttactggtcttcttttctttccA	rvs
5	NS2AB	CGCGTagcaagaaaaggagctggccattag	fwd
6		gatcctaatggccagctccttttcttgctA	rvs
7	NS2B3	CGCGTaagaaacaacgggccggagtattgg	fwd
8		gatcccaatactccggcccgttgtttcttA	rvs
9	NS3hel	CGCGTgcacaaagaagagggagaataggag	fwd
10		gatcctcctattctccctcttctttgtgcA	rvs
11	NS3prohel	CGCGTcgaaagagaagactgaccatcatgg	fwd
12		gatcccatgatggtcagtcttctctttcgA	rvs
13	panFlav	CGCGTggattgaaaagaggaggagcaaagg	fwd
14		gatccctttgctcctcctcttttcaatccA	rvs
15	ZV$_{opt}$	CGCGTaagaccggaaagagaagcggggcattag	fwd
16		gatcctaatgccccgcttctctttccggtcttA	rvs
17	nsp1/2	CGCGTgagctcaatggaggtgcagtcactcgctatg	fwd
18		gatccatagcgagtgactgcacctccattgagctcA	rvs
19	nsp2/3	CGCGTcgcttaaaaggggggtgcaccaattaaaggtg	fwd
20		gatccacctttaattggtgcacccccttttaagcgA	rvs
21	nsp3/4	CGCGTtcactcaagggtggtaagattgttagtactg	fwd
22		gatccagtactaacaatcttaccacccttgagtgaA	rvs
23	nsp4/5	CGCGTtctgctgttctgcagagtggtttttaggaaag	fwd
24		gatcctttcctaaaaccactctgcagaacagcagaA	rvs
25	nsp5/6	CGCGTggtgttaccttccaaggtaagttcaagaaag	fwd
26		GATCCtttcttgaacttaccttggaaggtaacaccA	rvs
27	nsp6/7	CGCGTgttgctactgtacagtctaaaatgtctgacg	fwd
28		gatccgtcagacattttagactgtacagtagcaacA	rvs
29	nsp7/8	CGCGTcgtgctactcttcaggctattgcttcagaag	fwd
30		gatccttctgaagcaatagcctgaagagtagcacgA	rvs
31	nsp8/9	CGCGTgctgttaaactacagaataatgaactgagtg	fwd
32		gatccactcagttcattattctgtagtttaacagcA	rvs
33	nsp9/10	CGCGTacagtacgtcttcaggctggaaatgctacag	fwd
34		gatcctgtagcatttccagcctgaagacgtactgtA	rvs
35	nsp10/RdRp	CGCGTgaacccttgatgcagtctgcggatgcatcag	fwd
36		gatcctgatgcatccgcagactgcatcaagggttcA	rvs
37	RdRp/Hel	CGCGTcatacagtcttgcaggctgtaggtgctgtg	fwd
38		gatccaaagcacctacagcctgcaagactgtatgA	rvs
39	Hel/nsp14	CGCGTgtggctcattacaagcagaaaatgtaactg	fwd
40		gatccagttacattttctgcttgtaatgtagccacA	rvs
41	nsp14/15	CGCGTtttaccaggttacagagtttagaaaatgtgg	fwd
42		gatcccacattttctaaactctgtaacctggtaaaA	rvs
43	nsp15/16	CGCGTctcaagcaagtcaagcgtggcaaccaggtg	fwd
44		gatccacctggttgccacgcttgacttgcttgtagA	rvs

[a]Capital letters indicate sequence noncomplementary to the reverse primer.
[b]fwd, forward; rvs, reverse.

confirmed by restriction pattern analysis and sequence analysis. The complete nucleotide and amino acid sequences of the reporter construct are available on request. The expression of the reporter construct was under the control of the eukaryotic translation elongation factor 1-alpha promoter.

Lentiviral transduction and generation of reporter cell lines. Cells stably expressing the protease reporter constructs were generated by lentiviral transduction. Subconfluent HEK-293T cells were transfected with the pWPI vector encoding the reporter construct together with packaging plasmids pCMV-Gag-Pol and pMD2-VSV-G (kind gifts from D. Trono, EPFL, Lausanne). After 2 days, the supernatant of the transfected cells was harvested, filtered, and stored at −80°C. Lentiviruses were titrated by SYBR green I-based real-time PCR-enhanced reverse transcriptase (SG-PERT) assay (46, 47) using the Takyon SYBR green kit (Eurogentec). The titer was determined by comparison with a standard curve of known RNA concentrations. Lentiviral transduction was performed by addition of the filtered supernatant to Huh7, Huh7-Lunet-T7, or A549-ACE2 cells (multiplicity of infection [MOI] = 5) in the presence of 4 µg/ml of Polybrene. For the generation of stable cell lines expressing the reporter constructs, cells were cultured in medium containing 1 µg/ml puromycin. Cells stably expressing the SARS-CoV-2-optimized reporter construct were selected by fluorescence-activated cell sorting (FACS) to obtain single-cell clones with homogenous expression levels of the fluorescent reporter.

Indirect immunofluorescence. Cells were seeded on glass coverslips and harvested at the indicated time points. The cells were washed once with phosphate-buffered saline (PBS) and fixed with paraformaldehyde (PFA) (4%) at room temperature (RT). PFA was removed, cells were washed once with PBS, and the coverslips were covered with PBS containing Triton X-100 (0.2%) to permeabilize the cells. Cells on coverslips were blocked with skim milk (2%) in PBS containing Tween 20 (PBS-T [0.02%]) for 1 h. After blocking, the coverslips were placed on 30 μl of primary antibody, diluted in the blocking buffer, with the cell side facing the drop. Cells were incubated for 1.5 h at RT and washed thrice with PBS-T (0.02%). The coverslips were then placed on 30 μl of secondary antibody with the cell side facing the drop. After 45 min of incubation at RT, the cells were washed thrice with PBS-T (0.02%) and coverslips were mounted on microscopy slides using Dapi-Fluoromount-G mounting media (Southern BioTech).

Western blotting. Cells were washed once with PBS and lysed in Western blot lysis buffer (1% Triton X-100). After sonication and denaturation at 95°C, the protein concentration was measured by Bradford assay. Cell lysates were mixed with Bradford reagent (1:5) and absorbance was measured at 595 nm. For each sample, 10 μg of total lysate was resolved by electrophoresis in a 10% or 15% sodium dodecyl sulfate-polyacrylamide gel for NS3 or GFP, respectively. Proteins were transferred to a polyvinylidene fluoride membrane overnight. Membranes were blocked in skim milk (5%) in PBS-T (0.2%) for 1 h at RT. After washing thrice with PBS-T (0.2%) for 15 min, membranes were incubated with primary antibody for 1 h at RT. The membranes were washed thrice and horseradish peroxidase (HRP)-conjugated secondary antibody was added. After incubation for 1 h at RT, the membrane was washed thrice and the bound antibodies were detected using enhanced chemiluminescence solution (Perkin Elmer, Waltham, MA, USA). Images were acquired using the ChemoCam 6.0 ECL system (INTAS Science Imaging, Goettingen, Germany).

Live cell imaging. Huh7-Lunet-T7 cells expressing the dengue reporter constructs (Lunet-T7-RC) were seeded onto a glass bottom 33 cm^2 dish (Mattek) at a density of 2×10^4. Transfection of the pIRO-D system (28) was performed at 24 h postseeding using the TransIT-LT1 (Mirus) transfection reagent according to the manufacturer's instructions. Four hours posttransfection (hpt) the transfection medium was exchanged for complete medium lacking phenol red (imaging medium). Images were collected with a Perkin Elmer spinning disk confocal microscope. For SARS-CoV-2 live cell imaging, A549-ACE2 or a selected clone of A549-ACE2 stably expressing the fluorescent reporter (A549-ACE2-RC), were seeded on 35-mm Ibidi dishes with gas permeable membrane and sealable lid. Cells were infected for 1 h with SARS-CoV-2 (MOI = 10) and at 2 hpi the medium was exchanged for imaging medium. The lid was moved to the locked position and silicon was used to seal the dish in order to prevent evaporation. Images were collected with a Nikon Eclipse Ti widefield microscope. Multiple observation fields were imaged for 8 h or 18 h at an interval of 10 min for transfection or infection, respectively.

Compound screening assay. A549-ACE2 reporter cells (clone C2) were seeded in duplicates for each condition. On the next day, the cells were treated with a 1:3 serial dilution, starting at 10 μM remdesivir, or with the solvent dimethyl sulfoxide (DMSO) serving as a control. After 30 min, cells were infected with SARS-CoV-2 (MOI = 5) in the presence of the compound for 2 h. Supernatants were aspirated and medium with compound was added to the cells. Supernatants were collected at 16 h postinfection and virus titers were determined by plaque assay. Infected cells were fixed with 6% paraformaldehyde and stained for N protein by IF. Images were acquired with a Perkin Elmer spinning disk confocal microscope. Signal intensity of N protein staining and nuclear GFP signal was quantified on a single cell level by a semiautomated image analysis workflow (32). Cells were considered infected when the signal intensity of nuclear GFP was higher than 7,000 arbitrary fluorescence units. Inhibition was quantified by normalizing the values to those obtained with cells that were treated with DMSO only (no inhibition). Alternatively, we quantified the number of cells with nuclear GFP using a semisupervised machine-learning pipeline based on CellProfiler and CellProfiler Analyst software, as described earlier (33). The software package is available upon request.

Bioinformatic analysis. Images were analyzed using the Fiji software (48, 49). Graph generation and statistical analysis was performed using the GraphPad Prism 8.1 software package. The scheme of the assumed reporter topology was designed with the Illustrate software (50) using the RCSD PDB entries 4EVL, 4RXH (chain A), 4CG5 (chain C), and 2VBC (chain B).

SUPPLEMENTAL MATERIAL

Supplemental material is available online only.
SUPPLEMENTAL FILE 1, PDF file, 0.2 MB.
SUPPLEMENTAL FILE 2, MP4 file, 3.3 MB.
SUPPLEMENTAL FILE 3, MP4 file, 1.3 MB.

ACKNOWLEDGMENTS

REFERENCES

1. Woolhouse MEJ, Brierley L. 2018. Epidemiological characteristics of human-infective RNA viruses. Sci Data 5:1–6. https://doi.org/10.1038/sdata.2018.17.
2. Pierson TC, Diamond MS. 2020. The continued threat of emerging flaviviruses. Nat Microbiol 5:796–812. https://doi.org/10.1038/s41564-020-0714-0.
3. Guzman MG, Harris E. 2015. Dengue. Lancet 385:453–465. https://doi.org/10.1016/S0140-6736(14)60572-9.
4. World Health Organization. 2018. Dengue vaccine: WHO position paper. World Health Organization 93:457–476.
5. Peiris JSM, Yuen KY, Osterhaus ADME, Stöhr K. 2003. The severe acute respiratory syndrome. N Engl J Med 349:2431–2441. https://doi.org/10.1056/NEJMra032498.
6. Zumla A, Hui DS, Perlman S. 2015. Middle East respiratory syndrome. Lancet 386:995–1007. https://doi.org/10.1016/S0140-6736(15)60454-8.
7. Lu R, Zhao X, Li J, Niu P, Yang B, Wu H, Wang W, Song H, Huang B, Zhu N, Bi Y, Ma X, Zhan F, Wang L, Hu T, Zhou H, Hu Z, Zhou W, Zhao L, Chen J, Meng Y, Wang J, Lin Y, Yuan J, Xie Z, Ma J, Liu WJ, Wang D, Xu W, Holmes EC, Gao GF, Wu G, Chen W, Shi W, Tan W. 2020. Genomic characterisation and epidemiology of 2019 novel coronavirus: implications for virus origins and receptor binding. Lancet 395:565–574. https://doi.org/10.1016/S0140-6736(20)30251-8.
8. Wu F, Zhao S, Yu B, Chen YM, Wang W, Song ZG, Hu Y, Tao ZW, Tian JH, Pei YY, Yuan ML, Zhang YL, Dai FH, Liu Y, Wang QM, Zheng JJ, Xu L, Holmes EC, Zhang YZ. 2020. A new coronavirus associated with human respiratory disease in China. Nature 579:265–269. https://doi.org/10.1038/s41586-020-2008-3.
9. World Health Organization. 2020. WHO coronavirus disease (Covid-19) dashboard. https://covid19.who.int/.
10. Welsch S, Miller S, Romero-Brey I, Merz A, Bleck CKE, Walther P, Fuller SD, Antony C, Krijnse-Locker J, Bartenschlager R. 2009. Composition and three-dimensional architecture of the dengue virus replication and assembly sites. Cell Host Microbe 5:365–375. https://doi.org/10.1016/j.chom.2009.03.007.
11. Knoops K, Kikkert M, Van Den Worm SHE, Zevenhoven-Dobbe JC, Van Der Meer Y, Koster AJ, Mommaas AM, Snijder EJ. 2008. SARS-coronavirus replication is supported by a reticulovesicular network of modified endoplasmic reticulum. PLoS Biol 6:e226. https://doi.org/10.1371/journal.pbio.0060226.
12. Neufeldt CJ, Cortese M, Acosta EG, Bartenschlager R. 2018. Rewiring cellular networks by members of the Flaviviridae family. Nat Rev Microbiol 16:125–142. https://doi.org/10.1038/nrmicro.2017.170.
13. Thiel V, Ivanov KA, Putics Á, Hertzig T, Schelle B, Bayer S, Weißbrich B, Snijder EJ, Rabenau H, Doerr HW, Gorbalenya AE, Ziebuhr J. 2003. Mechanisms and enzymes involved in SARS coronavirus genome expression. J Gen Virol 84:2305–2315. https://doi.org/10.1099/vir.0.19424-0.
14. Harcourt BH, Jukneliene D, Kanjanahaluethai A, Bechill J, Severson KM, Smith CM, Rota PA, Baker SC. 2004. Identification of severe acute respiratory syndrome coronavirus replicase products and characterization of papain-like protease activity. J Virol 78:13600–13612. https://doi.org/10.1128/JVI.78.24.13600-13612.2004.
15. Prentice E, McAuliffe J, Lu X, Subbarao K, Denison MR. 2004. Identification and characterization of severe acute respiratory syndrome coronavirus replicase proteins. J Virol 78:9977–9986. https://doi.org/10.1128/JVI.78.18.9977-9986.2004.
16. Ziebuhr J, Snijder EJ, Gorbalenya AE. 2000. Virus-encoded proteinases and proteolytic processing in the Nidovirales. J Gen Virol 81:853–879. https://doi.org/10.1099/0022-1317-81-4-853.
17. Cortese M, Goellner S, Acosta EG, Neufeldt CJ, Oleksiuk O, Lampe M, Haselmann U, Funaya C, Schieber N, Ronchi P, Schorb M, Pruunsild P, Schwab Y, Chatel-Chaix L, Ruggieri A, Bartenschlager R. 2017. Ultrastructural characterization of Zika virus replication factories. Cell Rep 18:2113–2123. https://doi.org/10.1016/j.celrep.2017.02.014.
18. Klein S, Cortese M, Winter SL, Wachsmuth-Melm M, Neufeldt CJ, Cerikan B, Stanifer ML, Boulant S, Bartenschlager R, Chlanda P. 2020. SARS-CoV-2 structure and replication characterized by in situ cryo-electron tomography. bioRxiv https://doi.org/10.1101/2020.06.23.167064.
19. McFadden MJ, Mitchell-Dick A, Vazquez C, Roder AE, Labagnara KF, McMahon JJ, Silver DL, Horner SM. 2018. A fluorescent cell-based system for imaging zika virus infection in real-time. Viruses 10:95–18. https://doi.org/10.3390/v10020095.
20. Hsieh MS, Chen MY, Hsieh CH, Pan CH, Yu GY, Chen HW. 2017. Detection and quantification of dengue virus using a novel biosensor system based on dengue NS3 protease activity. PLoS One 12:e0188170. https://doi.org/10.1371/journal.pone.0188170.
21. Medin CL, Valois S, Patkar CG, Rothman AL. 2015. A plasmid-based reporter system for live cell imaging of dengue virus infected cells. J Virol Methods 211:55–62. https://doi.org/10.1016/j.jviromet.2014.10.010.
22. Preugschat F, Yao CW, Strauss JH. 1990. In vitro processing of dengue virus type 2 nonstructural proteins NS2A, NS2B, and NS3. J Virol 64:4364–4374. https://doi.org/10.1128/JVI.64.9.4364-4374.1990.
23. Zhang R, Miner JJ, Gorman MJ, Rausch K, Ramage H, White JP, Zuiani A, Zhang P, Fernandez E, Zhang Q, Dowd KA, Pierson TC, Cherry S, Diamond MS. 2016. A CRISPR screen defines a signal peptide processing pathway required by flaviviruses. Nature 535:164–168. https://doi.org/10.1038/nature18625.
24. Arias CF, Preugschat F, Strauss JH. 1993. Dengue 2 virus NS2B and NS3 form a stable complex that can cleave NS3 within the helicase domain. Virology 193:888–899. https://doi.org/10.1006/viro.1993.1198.
25. Nestorowicz A, Chambers TJ, Rice CM. 1994. Mutagenesis of the yellow fever virus NS2A/2B cleavage site: effects on proteolytic processing, viral replication, and evidence for alternative processing of the NS2A protein. Virology 199:114–123. https://doi.org/10.1006/viro.1994.1103.
26. Westaway EG, Mackenzie JM, Kenney MT, Jones MK, Khromykh AA. 1997. Ultrastructure of Kunjin virus-infected cells: colocalization of NS1 and NS3 with double-stranded RNA, and of NS2B with NS3, in virus-induced membrane structures. J Virol 71:6650–6661. https://doi.org/10.1128/JVI.71.9.6650-6661.1997.
27. Schmid B, Rinas M, Ruggieri A, Acosta EG, Bartenschlager M, Reuter A, Fischl W, Harder N, Bergeest JP, Flossdorf M, Rohr K, Höfer T, Bartenschlager R. 2015. Live cell analysis and mathematical modeling identify determinants of attenuation of dengue virus 2'-O-methylation mutant. PLoS Pathog 11:e1005345. https://doi.org/10.1371/journal.ppat.1005345.
28. Cerikan B, Goellner S, Neufeldt CJ, Haselmann U, Mulder K, Chatel-Chaix L, Cortese M, Bartenschlager R. 2020. A non-replicative role of the 3' terminal sequence of the dengue virus genome in membranous replication organelle formation. Cell Rep 32:107859–107859. https://doi.org/10.1016/j.celrep.2020.107859.
29. Neufeldt CJ, Cerikan B, Cortese M, Frankish J, Lee J-Y, Plociennikowska A, Heigwer F, Joecks S, Burkart SS, Zander DY, Gendarme M, Debs BE, Halama N, Merle U, Boutros M, Binder M, Bartenschlager R. 2020. SARS-CoV-2 infection induces a pro-inflammatory cytokine response through cGAS-STING and NF-kB. bioRxiv https://doi.org/10.1101/2020.07.21.212639:2020.07.21.212639-2020.07.21.212639.
30. Xie X, Muruato AE, Zhang X, Lokugamage KG, Fontes-Garfias CR, Zou J, Liu J, Ren P, Balakrishnan M, Cihlar T, Tseng C-TK, Makino S, Menachery VD, Bilello JP, Shi P-Y. 2020. A nanoluciferase SARS-CoV-2 for rapid neutralization testing and screening of anti-infective drugs for COVID-19. bioRxiv https://doi.org/10.1101/2020.06.22.165712:2020.06.22.165712-2020.06.22.165712.
31. Pruijssers AJ, George AS, Schafer A, Leist SR, Gralinksi LE, Dinnon KH, 3rd, Yount BL, Agostini ML, Stevens LJ, Chappell JD, Lu X, Hughes TM, Gully K, Martinez DR, Brown AJ, Graham RL, Perry JK, Du Pont V, Pitts J, Ma B, Babusis D, Murakami E, Feng JY, Bilello JP, Porter DP, Cihlar T, Baric RS, Denison MR, Sheahan TP. 2020. Remdesivir inhibits SARS-CoV-2 in human lung cells and chimeric SARS-CoV expressing the SARS-CoV-2 RNA polymerase in mice. Cell Rep 32:107940. https://doi.org/10.1016/j.celrep.2020.107940.

32. Pape C, Remme R, Wolny A, Olberg S, Wolf S, Cerrone L, Cortese M, Klaus S, Lucic B, Ullrich S, Anders-Össwein M, Wolf S, Berati C, Neufeld C, Ganter M, Schnitzler P, Merle U, Lusic M, Boulant S, Stanifer M, Bartenschlager R, Hamprecht FA, Kreshuk A, Tischer C, Kräusslich H-G, Müller B, Laketa V. 2020. Microscopy-based assay for semi-quantitative detection of SARS-CoV-2 specific antibodies in human sera. bioRxiv https://doi.org/10.1101/2020.06.15.152587:2020.06.15.152587-2020.06.15.152587.

33. Prasad V, Suomalainen M, Hemmi S, Greber UF. 2017. Cell cycle-dependent kinase Cdk9 is a postexposure drug target against human adenoviruses. ACS Infect Dis 3:398–405. https://doi.org/10.1021/acsinfecdis.7b00009.

34. Arias-Arias JL, MacPherson DJ, Hill ME, Hardy JA, Mora-Rodríguez R. 2020. A fluorescence-activatable reporter of flavivirus NS2B–NS3 protease activity enables live imaging of infection in single cells and viral plaques. J Biol Chem 295:2212–2226. https://doi.org/10.1074/jbc.RA119.011319.

35. Chatel-Chaix L, Cortese M, Romero-Brey I, Bender S, Neufeldt CJ, Fischl W, Scaturro P, Schieber N, Schwab Y, Fischer B, Ruggieri A, Bartenschlager R. 2016. Dengue virus perturbs mitochondrial morphodynamics to dampen innate immune responses. Cell Host Microbe 20:342–356. https://doi.org/10.1016/j.chom.2016.07.008.

36. Xie X, Muruato A, Lokugamage KG, Narayanan K, Zhang X, Zou J, Liu J, Schindewolf C, Bopp NE, Aguilar PV, Plante KS, Weaver SC, Makino S, LeDuc JW, Menachery VD, Shi PY. 2020. An infectious cDNA clone of SARS-CoV-2. Cell Host Microbe 27:841–848. https://doi.org/10.1016/j.chom.2020.04.004.

37. Thi Nhu Thao T, Labroussaa F, Ebert N, V'kovski P, Stalder H, Portmann J, Kelly J, Steiner S, Holwerda M, Kratzel A, Gultom M, Schmied K, Laloli L, Hüsser L, Wider M, Pfaender S, Hirt D, Cippà V, Crespo-Pomar S, Schröder S, Muth D, Niemeyer D, Corman VM, Müller MA, Drosten C, Dijkman R, Jores J, Thiel V. 2020. Rapid reconstruction of SARS-CoV-2 using a synthetic genomics platform. Nature 582:561–565. https://doi.org/10.1038/s41586-020-2294-9.

38. Hou YJ, Okuda K, Edwards CE, Martinez DR, Asakura T, Dinnon KH, Kato T, Lee RE, Yount BL, Mascenik TM, Chen G, Olivier KN, Ghio A, Tse LV, Leist SR, Gralinski LE, Schäfer A, Dang H, Gilmore R, Nakano S, Sun L, Fulcher ML, Livraghi-Butrico A, Nicely NI, Cameron M, Cameron C, Kelvin DJ, de Silva A, Margolis DM, Markmann A, Bartelt L, Zumwalt R, Martinez FJ, Salvatore SP, Borczuk A, Tata PR, Sontake V, Kimple A, Jaspers I, O'Neal WK, Randell SH, Boucher RC, Baric RS. 2020. SARS-CoV-2 reverse genetics reveals a variable infection gradient in the respiratory tract. Cell 182:429–446. https://doi.org/10.1016/j.cell.2020.05.042.

39. Wang M, Cao R, Zhang L, Yang X, Liu J, Xu M, Shi Z, Hu Z, Zhong W, Xiao G. 2020. Remdesivir and chloroquine effectively inhibit the recently emerged novel coronavirus (2019-nCoV) in vitro. Cell Res 30:269–271. https://doi.org/10.1038/s41422-020-0282-0.

40. Bykov YS, Cortese M, Briggs JAG, Bartenschlager R. 2016. Correlative light and electron microscopy methods for the study of virus–cell interactions. FEBS Lett 590:1877–1895. https://doi.org/10.1002/1873-3468.12153.

41. Froggatt HM, Heaton BE, Heaton NS. 2020. Development of a fluorescence based, high-throughput SARS-CoV-2 3CLpro reporter assay. bioRxiv https://doi.org/10.1101/2020.06.24.169565.

42. Nakabayashi H, Miyano K, Sato J, Yamane T, Taketa K. 1982. Growth of human hepatoma cell lines with differentiated functions in chemically defined medium. Cancer Res 42:3858–3863.

43. Friebe P, Boudet J, Simorre J-P, Bartenschlager R. 2005. Kissing-loop interaction in the 3′ end of the hepatitis C virus genome essential for RNA replication. J Virol 79:380–392. https://doi.org/10.1128/JVI.79.1.380-392.2005.

44. Appel N, Pietschmann T, Bartenschlager R. 2005. Mutational analysis of hepatitis C virus nonstructural protein 5A: potential role of differential phosphorylation in RNA replication and identification of a genetically flexible domain. J Virol 79:3187–3194. https://doi.org/10.1128/JVI.79.5.3187-3194.2005.

45. Fischl W, Bartenschlager R. 2013. High-throughput screening using dengue virus reporter genomes. Methods Mol Biol 1030:205–219. https://doi.org/10.1007/978-1-62703-484-5_17.

46. Pizzato M, Erlwein O, Bonsall D, Kaye S, Muir D, McClure MO. 2009. A one-step SYBR Green I-based product-enhanced reverse transcriptase assay for the quantitation of retroviruses in cell culture supernatants. J Virol Methods 156:1–7. https://doi.org/10.1016/j.jviromet.2008.10.012.

47. Vermeire J, Naessens E, Vanderstraeten H, Landi A, Iannucci V, van Nuffel A, Taghon T, Pizzato M, Verhasselt B. 2012. Quantification of reverse transcriptase activity by real-time PCR as a fast and accurate method for titration of HIV, lenti- and retroviral vectors. PLoS One 7:e50859. https://doi.org/10.1371/journal.pone.0050859.

48. Schindelin J, Arganda-Carreras I, Frise E, Kaynig V, Longair M, Pietzsch T, Preibisch S, Rueden C, Saalfeld S, Schmid B, Tinevez JY, White DJ, Hartenstein V, Eliceiri K, Tomancak P, Cardona A. 2012. Fiji: an open-source platform for biological-image analysis. Nat Methods 9:676–682. https://doi.org/10.1038/nmeth.2019.

49. Schneider CA, Rasband WS, Eliceiri KW. 2012. NIH Image to ImageJ: 25 years of image analysis. Nat Methods 9:671–675. https://doi.org/10.1038/nmeth.2089.

50. Goodsell DS, Autin L, Olson AJ. 2019. Illustrate: software for biomolecular illustration. Structure 27:1716–1720. https://doi.org/10.1016/j.str.2019.08.011.

51. Shiryaev SA, Kozlov IA, Ratnikov BI, Smith JW, Lebl M, Strongin AY. 2007. Cleavage preference distinguishes the two-component NS2B-NS3 serine proteinases of dengue and West Nile viruses. Biochem J 401:743–752. https://doi.org/10.1042/BJ20061136.